Published in final edited form as:
Arterioscler Thromb Vasc Biol. 2011 June ; 31(6): 1351–1356. doi:10.1161/ATVBAHA.111.225334.

In Vivo Fluorescence Imaging of Large-Vessel Thrombosis in Mice

Brian C. Cooley, Ph.D.
Medical College of Wisconsin, 8701 Watertown Plank Road, Milwaukee, WI 53226, Phone: 414-456-8729

Brian C. Cooley: bcooley@mcw.edu

Abstract

Objectives—Experimental studies of large-vessel thrombosis have been adapted for applications in mice, but proffer limited quantifiable information in outcome measures. This study presents a novel approach for evaluating large-vessel thrombogenesis with temporally/spatially quantifiable measures and normalization methods for inter-animal comparisons.

Methods and Results—Shuttered, beam-expanded lasers provided uniform narrow-wavelength illumination of a 100× microsurgical field with large depth of focus. Thrombosis was generated in murine carotid arteries and femoral veins by brief vascular surface electrolytic injury. Thrombus-targeting fluorophores were injected systemically and subsequently localized at the site of thrombus induction. A low-light digital video camera with filter wheel provided target-specific image acquisition over a 60-minute interval. Platelets accumulated with a subsequent fibrin border emerging to stabilize the clot in both arteries and veins. Coagulation enzyme complexes colocalized with fibrin deposition. Large arteries underwent cyclic massive thrombo-embolization, whereas veins showed gradual shedding of microemboli and clot contraction. Systemic administration of fibrin- and platelet-inhibiting compounds reduced their respective targets, but also often inhibited their clotting counterparts (platelets and fibrin, respectively) in both arteries and veins.

Conclusions—Intermediate-level magnified image capture represents a novel approach for analysis of fluorescence-based in vivo imaging, with quantitative application to the study of large-vessel thrombosis.

Keywords

thrombosis; artery; vein; platelets; fibrin

Introduction

Studies seeking to understand the basis of thrombosis or to evaluate antithrombotic therapies have increasingly turned to murine systems, exploiting the capacity for genetic manipulations of the mouse genome to dissect the roles of various proteins and related factors on in vivo clot formation. Experimental thrombosis models in mice, however, have outcome measures that offer little informational content, due in part to the restrictions of working with the very small vascular structures inherent to this species. Large-artery thrombosis studies have most often applied measures of the time to occlusion after a free radical-mediated injury (usually applying topical $FeCl_3$[1] or using laser irradiation with

Disclosure: The authors has no conflicts of interest related to this work.

circulating Rose bengal for photochemical induction of localized free radicals[2-3]). Many venous thrombosis models rely on vascular occlusion, via total or partial ligation of the vena cava, with subsequent measurement of stasis-induced clot weight, dimensions, or other properties at a fixed time after clot induction. These models may not accurately simulate clotting phenomena of relevance to clinical thrombosis: a site of thrombotic activity with maintained flow for which the therapeutic intent is to minimize thrombotic growth and/or embolization and to prevent subsequent vascular occlusion.

In the past several years, elegant in vivo thrombosis imaging systems have been developed,[4-6] using thin-tissue structures that are adaptable to microscopic viewing, and which incorporate fluorescent probes for specific cellular- and molecular-targeted imaging. These studies have provided insight into how intravascular blood clots form in microvessels; however, they address neither large-vessel thrombosis nor microvessel hemostasis (cessation of bleeding in transected microvessels). Furthermore, the mechanisms for generating blood clot formation in these systems, most often using broad-surface perfusion with free-radical generating solutions or laser-photonic heat injuries, have qualified clinical relevance. Many early studies of large-vessel thrombosis used circulating radiolabeled platelets and fibrinogen to identify and quantitate clot development,[7,8] however, these experiments suffer from poor spatial resolution and related shortcomings (e.g., labeled fibrinogen does not distinguish fibrin-clotted versus platelet-bound fibrinogen in the clot). The study of large-vessel thrombosis would greatly benefit from the high temporal and spatial resolution of the recently developed microvessel imaging systems.

To this end, an imaging system was developed for evaluating in vivo large-vessel thrombosis which uses moderate magnification (100×) with increased depth of focus (for larger vessels), a beam-expanded and shuttered laser array for uniform field illumination with narrow bandwidths to stimulate fluorophore excitation, and specific sets of fluorophores linked to clot-targeting molecules and cells to achieve quantifiable measures of multiple targets in the same clot site. Thrombus induction was generated by electrolytic injury via iron ion shedding to a discrete spot on the vessel surface, controlled by voltage and application time to yield reproducible subsequent thrombogenesis. A normalization procedure was developed to permit direct and highly quantitative inter-animal comparisons of thrombus element localization within the site.

Methods

Imaging System (Figure 1)

An array of three lasers – 532 nm, 594 nm, and 650 nm – with power levels of 10-40 mW were beam-expanded to approximately 1 cm diameters and aimed to converge (after downward mirror reflection) on a microsurgical field of an exposed surgical site in an anesthetized mouse. A Wild/Leica operating microscope with 100-mm objective lens viewed the field and was mounted with a DVC-1412 low-light digital video camera and filter wheel (DVC, Inc., Austin, Texas). The laser paths passed through a camera-synchronized Uniblitz shutter (Vincent Associates, Ottawa, Canada). Emission filters of 555-575 nm, 614-645 nm, and 696-730 nm (Chroma Technology, Inc., Bellows Falls, Vermont) permitted yellow, red, and near-infrared fluorophore-specific image capture, with camera exposure times of 0.1 – 1.0 seconds; between-exposure delays up to 10 seconds allowed time-lapse video imaging for up to 60 minutes. The camera field of microscopic view at highest magnification was 2.4 × 3.2 mm and was evenly illuminated with each of the defocused laser beams. The total power density of continuous laser irradiation was approximately 20% of that provided by the standard white light illumination of the microscope, with minimal heating effects on the surgical field; the shuttering feature also helped minimized radiative heat generation from the lasers.

Fluorescent Labels and Antithrombotic Compounds

Platelets were isolated from donor mouse blood anticoagulated with acid-citrate-dextrose and labeled ex vivo with Vybrant DiD (Invitrogen). Alternatively, platelets were labeled in vivo by injection of Rhodamine 6G (100 μL, 1 mM concentration). Antibodies, human fibrinogen, and activated protein C were labeled with Alexa-Fluor-532, -594, or -647 using standard kits (Invitrogen). A monoclonal antibody specific for fibrin[9-10] was isolated from ascites from a hybridoma clone (59D8) kindly provided by Dr. Marschall Runge; other antibodies included those for mouse Factor VIII/VIIIa, IX/IXa, and X/Xa (Haematologic Technologies, Essex Junction, Vermont) and P-selectin (Chemicon/Millipore, Billerica, CA). An antibody specific for the activated platelet receptor αIIb/β3 (JON/A) was pre-labeled with phycoerythrin (Emfret, Eibelstadt, Germany).

Antithrombotic agents were administered independently of the fluorophore/platelet injections at concentrations comparable to clinically relevant doses: heparin (i.v., 200 units/kg), hirudin (i.v., 1 mg/kg), aspirin (intragastrically 4 hours prior to thrombus induction, 15 mg/kg), and clopidogrel (intragastrically 24 and again 4 hours prior to thrombus induction, 10 mg/kg).

Surgery and Thrombosis Models

All animal studies were done under Medical College of Wisconsin Institutional Animal Care and Use Committee-approved protocols. Wild-type C57Bl/6 mice were purchased from Harlan SD (Indianapolis, IN) and Factor IX-null mice were from Jackson Laboratories (Bar Harbour, ME). Factor VIII-null mice were kindly supplied by Dr. Haig Kazazian and Factor V Leiden mice were from Dr. David Ginsburg. Mice were anesthetized with intraperitonal pentobarbital (50 mg/kg) with maintenance dosing as required. Simple skin incisions permitted vessel exposures of the jugular vein (for intravenous injections), and of the carotid arteries, (with an external diameter of 0.3-0.5 mm) and femoral veins (diameter, 0.5-1.0 mm). Labeled platelets (up to 1×10^7 injected per mouse) or fluorophore-labeled antibodies/proteins were injected into the jugular vein in volumes up to 100 μL, 3-5 minutes prior to thrombus induction; labeled anti-fibrin was used in the quantitative studies at amounts of 10-20 μg per mouse. Electrolytic injuries were induced on the surface of the carotid artery with a 30-second, 3-volt direct current application, touching the surface of the vessel with the blunt end of a 140-micron-diameter steel needle (Surgical Specialties Inc., Reading, PA) connected to the anode, completing the circuit by contacting local subdermal tissue with the cathode. A similar injury was made on the femoral vein, touching the surface for 30 seconds, 1.5 volts, with a 70-micron blunt-end needle. Applications under similar conditions with wires of copper, zinc, silver, or titanium did not yield detectable clots, supporting an iron ion-mediated electrolytic injury of clot induction, operating similarly as ferric chloride models of clot induction.[3,4] A modified $FeCl_3$ model was also used for comparison: the corner of a piece of filter paper soaked in a 20% $FeCl_3$ solution was touched to the surface of the carotid artery for 30 seconds, comparable to the contact time and footprint used for the electrolytic injuries. Several other methods of thrombus induction were evaluated, which showed less consistency; these are described and presented in the Supplemental Section.

Fluorophore Normalization

Primary measures for most experiments used platelets and anti-fibrin, labeled with distinct fluorophores. Labeled compounds were injected in a 100-μL volume through a branch of the jugular vein. A 1-uL volume of the fluorophore-containing injectate was spotted on a slide and imaged under the same laser illumination and magnification conditions used for the in vivo experiment; the total intensity of each fluorophore was thus determined: [fluorescence intensity of 1 uL] × [100 (injectate volume in uL)] = [total injected fluorescence under identical imaging conditions]. For each clot, the pixel intensity within the area of clotting

activity was measured, with background subtraction, on temporally spaced images of a time-lapse video. A comparative index of measure was developed to normalize experimental runs, controlling for the injected amount of each fluorophore, the labeled intensity of the fluorophore-bound targeting molecule/cell, and the animal weight:

[Area of Thrombus] × [(Average Pixel Intensity for a Given Flurophore) – (Background Intensity)] × [Animal Weight Ratio Adjustment Factor] / [Total Injected Fluorophore Intensity (determined under same imaging conditions)] = Normalized Intensity Index (of a given fluorophore within the clot)

The Animal Weight Ratio Adjustment Factor is defined as the reciprocal of the animal weight divided by 25 grams, a non-parametric constant approximately inversely proportional to the blood volume of each animal, and thus, the final concentration of circulating fluorophore available to interact with the thrombus over time.

Each clot had a measured fluorophore intensity under 3 times that of the 1 uL spotted injectate, thus, the clots had less than 3% of the total circulating fluorescence potential, implying a relatively low dilutional factor of fluorophore-linked targeting cell/molecule as it became incorporated into the clot.

To validate the approach, series of clots were generated by varying induction conditions and harvested immediately after imaging, measuring and summing normalized intensities of platelets and fibrin, the two dominant components of a thrombus. The harvested clots then underwent histomorphometric volume reconstruction.[11] The comparative results show a high degree of linear correlation (Pearson correlation coefficient, r = 0.915; Supplemental Fig. I).

Results

Iron-based electrolytic injury to the vessel surface led to non-occlusive accumulation of substantial amounts of both platelets and polymerizing fibrin localized to the site of injury (Fig. 2a,b). Progressive clot growth was evident starting immediately after thrombus induction and peaking at greater than 10 minutes in both arteries and veins. Intriguingly, both clotting elements showed prominent accumulation in both vessel types (Fig. 2c,d). This is in contrast to the accepted finding that platelets dominate the “white” clot of arteries and that fibrin is the more operational component of the “red” clot in veins.

The rate of clot dissolution showed dramatically different patterns between the vessel types. Arterial thrombi often underwent massive and occasionally near-total embolization (Fig. 2a; minute 37), followed by regrowth, sometimes with repeated embolization over a 60-minute observation period (Supplemental Video 1). Furthermore, the extent of platelet versus fibrin embolization was non-uniform (Fig. 2a; minute 21 vs. 37). In contrast to arterial thrombosis, clots within veins displayed a more gradual shedding of thrombus, via micro-emboli, and always maintained the bulk of the clot attached to the injury site for the duration of observation (Supplemental Video 2).

Application of $FeCl_3$ to the vessel surface in a more localized region (by touching the corner of the $FeCl_3$-saturated filter paper to the vessel for 30 seconds) generated subsequent non-occlusive thrombogenesis with temporal, spatial, and compositional characteristics very similar to the electrolytic injuries (Supplemental Video 3). This suggests that the occlusive thrombus, created by the more standardized model of onlaying a larger piece of $FeCl_3$-saturated filter paper for longer times, undergoes similar but more intense thrombogenic activity, leading to vascular occlusion. Evaluation of vessels treated more standardly with $FeCl_3$ led to early occlusion (under 12 minutes) and little change in thrombotic element

development at the site thereafter, thus yielding little further informational value following the occlusive event (data not shown). The lesser $FeCl_3$ injury, while non-occlusive and continually dynamic, was technically less reproducible than the electrolytic injury model. Similar lack of reproducibility was found for several other thrombus induction models (Supplemental Section), though in general, similar involvement of both platelets and fibrin in both arterial and venous thrombi were seen.

Distinct patterns emerged for the specific localization of a number of clot-targeting elements under the electrolytic injury. Platelets tended to accumulate in a relatively homogenous mass attached to the clot induction site, sometimes showing a gradual downstream “drift” in localization that often preceded large and small embolic events in arteries and veins, respectively. Fibrin-specific labeled antibodies localized to a shell-like perimeter that coincided with the apparent dimensions of the injury zone, often with substantially less evident fibrin accrual over the central injury zone, for both arteries and veins (Supplemental Fig. IIa). The same differential localization of platelets and fibrin was seen when fluorescent bandwidths were reversed for each thrombus marker (e.g., anti-fibrin labeled with Alexa-532 vs. -647; platelets labeled with Vybrant DiD (red) vs. rhodamine 6G (green)). The intensity of this fibrin border increased over time and appeared to serve as a stabilizing structure, securing the platelet thrombus to the vessel wall and inhibiting platelet embolization. To what molecular or cellular components this fibrin attaches will require further study. Labeled fibrinogen had an intermediate localization seen in large amounts both in fibrin-low/platelet-rich regions and in fibrin-dense sites, in both arteries and veins, consistent with its dual role in platelet aggregation and fibrin clot formation (Supplemental Fig. IIa).

Labeled antibodies specific for Factors VIII/VIIIa, IX/IXa, or X/Xa slightly preceded and spatially colocalized with fibrin-dense regions in both veins and arteries (Supplemental Fig. IIb and III). Labeled activated protein C, a natural inhibitor of both Factor Va (of the Va/Xa complex) and Factor VIIIa (of the VIIIa/IXa complex), when used in low concentrations that did not inhibit clot formation, followed a similar colocalization pattern to fibrin as with the VIII/VIIIa, IX/IXa, and X/Xa antibodies (data not shown). Intriguingly, a fluorophore prone to photobleaching and attached to an antibody specific to the activated form of αIIb/β3 (JON/A, Emfret), when used with unblocked laser illumination to promote photobleaching, revealed late-developing small platelet masses in large-vein clots that appeared to roll in the direction of flow along the outer border of the established platelet mass, embolizing at the tail of the clot (Supplemental Video 4). This finding is consistent with recent studies[12-13] that show surface rolling or loose adherence by small platelet masses and reveals the dynamic nature of platelet activity within ongoing thrombogenic stimuli.

Several standard antithrombotic agents were evaluated under both arterial and venous thrombosis conditions using the described imaging system. A method for quantitatively normalizing the amount of clotting element was applied, to enable direct comparisons among experimental groups. High therapeutic levels of heparin and hirudin, well-established inhibitors of fibrin clotting which function primarily by blocking thrombin activity, lead to an approximately 10-fold reduction of fibrin in both veins and arteries, and similar platelet reduction in veins and at early time points in arteries (solid black vs. light and dark gray lines in Fig. 3a-d). Knockout mouse lines for Factors VIII and IX each showed dramatic reductions in both clotting components (Fig. 3e,f). The Factor V Leiden mutation in humans is a strong risk factor for deep vein thrombosis;[14-15] the mutated Factor Va protein is less effectively inhibited by activated protein C. A mutant Factor V transgenic mouse[16], with single amino acid change analogous to the human Factor V Leiden gene mutation, showed larger clots with elevated amounts of both fibrin and platelets (Fig. 3e,f). Inhibition of a number of platelet activating receptors can reduce platelet aggregation in vitro and in vivo.

Aspirin and clopidogrel, two commonly used inhibitors of platelet activation and aggregation (through the thromboxane and $P2Y_{12}$ receptor pathways, respectively), reduced platelet accumulation in both vessel types; fibrin formation was also inhibited but to a lesser extent (Fig. 3a-d). These findings are consistent with central roles of thrombin (for fibrin formation and platelet activation) and platelets (for aggregation and surface-mediated coagulation complex assembly), and furthermore, they underscore the interactive role of fibrin and platelets in blood clot development and stabilization within large vessels.

Discussion

This quantitative, highly informative imaging system provides a unique platform by which to query thrombotic activities under a variety of circumstances. The use of multiple clot-targeting, fluorescently identifiable moieties in the same experimental preparation expands the repertoire of what can be studied in a single experiment. Using independent labels for platelets and fibrin, the dominant components of clots, provides a means for comparative quantitation of thrombogenesis. The resolution of this imaging system, down to 2-by-2 microns per pixel (with higher resolution possible using higher-end cameras), permits spatial discrimination of many dynamic clotting events, including micro-embolism and clot contraction. Furthermore, time-lapse video replay gives a unique perspective on otherwise slow-developing thrombodynamic activities.

Several novel features of large-vessel thrombosis become evident through this imaging approach. Arterial thrombo-embolic events are common (Fig. 2a), often occurring at later time points and occasionally seen to have highly repetitive regrowth and re-embolization. Platelets and fibrin do not consistently embolize and regrow to the same extent. Venous thrombi have a more stable growth, usually with only small embolic events seen after peak growth (Fig. 2b). The differences in embolic quality are likely due to the higher shear forces under arterial flow conditions. Clot contracture can also be observed, appearing as a consolidation of the clot around its vessel wall attachment site. This bulk change through clot contracture was only clearly evident in venous, not arterial, thrombi, and only occasionally seen; the mechanism of this contractile action is currently under investigation. Coagulation factors appear more densely in colocalization with fibrin-intense regions, but only slightly preceding fibrin formation in these localized densities (Supplemental Fig. II and III). Despite potential differences in attenuation rates for different fluorophores, creation of a thrombotic nidus on the topmost portion of the vessel surface, directly imaged by the camera/microscope, minimized these attenuation effects (Supplemental Fig. IV), thus permitting relatively accurate measurement and quantitation of these clotting events. The normalization approach for data analysis has reasonable linearity with moderate changes in the amount of injected fluorophore, whether this variation was due to altered levels of fluorophore incorporation in the target during its preparation or to the total amount of injected fluorophore-bound targeting cell/molecule. The resulting image intensity, which is proportional to the injected fluorophore intensity, is thus normalized offline through calculation, allowing inter-animal quantitative comparisons of clotting components.

Other microscopic methods of murine in vivo thrombus imaging have been developed, primarily designed for and applied to thrombi induced in microvessels. Rosen and colleagues[5] used laser irradiation alone or in combination with circulating Rose bengal to generate thrombi in mouse ear vessels; thrombi were directly imaged with incident light. Fluorescence microscopy has been used to image mesenteric[4] or cremaster[6] preparations, with thrombus induction within arterioles/venules by ferric chloride superfusion[4] or laser spot injury,[6] respectively. The fluorophore-tagging methodologies of the current report were adapted from those described in these earlier studies, using a similar ex vivo platelet-labeling strategy[4] and thrombus-targeted antibodies labeled with selected fluorophores.[6]

Whereas these microvessel imaging models can use the shorter excitation/emission wavelengths of calcein AM (for platelet labeling[4]) and Alexa-350 and -488 for antibody labeling,[6] due to the thin tissues studied, these fluorophores are more strongly attenuated by the thicker tissues and clots of large-vessel thrombosis evaluation, necessitating a shift to longer-wavelength-activated fluorophores described in the current report.

A major difference between the results presented in this report and findings from microvessel thrombus analyses is the time course of thrombogenesis. Site-localized thrombus induction by laser injury[5,6] generates rapid clot growth, generally seen to reach peak activity in 60 to 90 seconds. Superfused ferric chloride also causes faster thrombus growth,[4] with peak growth more difficult to ascertain (possibly due to the non-localization of induction) but appearing to be under 10 minutes. In contrast, the electrolytic injuries applied herein displayed more prolonged growth kinetics, usually peaking at greater than 10 minutes in arteries and more than 20 minutes in veins (Figure 3). This occurred regardless of inhibitor effects, supporting a general time course for this thrombus induction model. Mechanical injury (with apparent intravascular collagen exposure) showed shorter times to peak growth,(Supplemental Figure V) but the general time course was still considerably longer than in microvessel thrombus systems. These longer times may be due to one or more factors: 1) sustained thrombotic stimulation, 2) a cumulative synergism related to the net (i.e., larger) surface area of thrombus induction, 3) flow-mediated effects in larger vessels, or 4) greater intravascular extension of the thrombus into the lumen; a combination of more than one of these factors is likely to be operative, but will require further study.

Pharmacologic control of thrombosis has been a continuously active area of research since the emergence of heparin to reduce venous thromboembolism over 70 years ago.[17-18] The long-held view, that platelets are more responsible for arterial thrombosis while fibrin clotting is central to large vein thrombosis, has been based on a variety of in vitro and in vivo experiments, post-mortem analyses, and many clinical trials. This has guided most approaches to clinical therapies, with some notable exceptions. For example, vascular surgeons still typically use heparin-based compounds to inhibit fibrin clotting when undertaking many arterial-repair procedures (where platelets are expected to be more thrombotically operative) and debate is still open about the effects of platelet-inhibiting agents on venous thromboembolism. Post-mortem studies of both coronary artery[19] and deep vein thrombosis[20] have found variability, too, with regions of high platelet content (white clot) as well as other regions of fibrin-entrapped red blood cells (red clot) in both arteries and veins. The results herein support this overlap of platelets and fibrin within both arterial and venous thrombi. This unique finding may be dependent upon the specific model of thrombus induction (i.e., electrolytic injury), and thus, may be a limitation of the application of this model to the comparison of platelets and fibrin within a thrombus. However, other models of thrombus induction were evaluated and found to yield various degrees of dual platelet/fibrin accumulation (Supplemental Figure V). A better understanding of how thrombogenesis progresses and the effects of various pharmacologic agents on these processes is still needed to advance therapeutic care.

Blood clot imaging with current fluorophore-based approaches has limitations in terms of depth of field (red blood cells attenuate all wavelengths, particularly those less than 660 nm), 3-dimensional profile (with the depth dimension approximated by pixel intensity measurement of the 2-dimensional captured image), and precision (red and infrared wavelengths have lower scatter in biologic tissues, but their low attenuation leads to significant levels of marginal diffusion that can reduce the precise determination of spatial localization). Despite these drawbacks, the system and approach presented herein provide a substantial improvement over previous quantitative methodologies. Platelets and fibrin, the principal components of intravascular clots, can be quantitated over 2 orders of magnitude,

for comparisons ranging from extremely hypothrombotic phenotypes (e.g., hemophilia models) to more prothrombotic conditions. A limitation of the study is the time lag between thrombus induction and the first useful data point (2 minutes in the presented data). This lag leads to a “blind spot” in early thrombotic events with this imaging approach, which is evident by the differences in starting values among the pharmacologically inhibited experimental conditions in Figure 3.

The system as described used inexpensive components and relatively low-power lasers with long (up to 1 second) camera exposure times. The components of the described system, minus the microscope, were purchased for under $20,000, with most of this cost (~$16,000) represented by the low-light camera/filter-wheel. The red and green lasers, the mirror, and the filters can be purchased for relatively low cost with thrifty shopping, with adaptation to an existing dissecting/operating microscope/camera system, to assemble a functional system cost-effectively. Higher-end cameras and more powerful lasers can be employed to permit shorter exposure times which would substantially improve resolution without tissue heating or other modulatory effects. Thus, by customizing the system assembly, specific experimental needs of a laboratory can be met within budgetary constraints. A cautionary word is in order with regard to inherent safety issues with use of Class IIIb and IV lasers (above 5 mW for most visible wavelengths); until a laser beam enters a beam-expanding lens, its power density presents an eye hazard to experimenters and research animals, so following proper laser safety procedures is essential.

In summary, this approach to large-vessel thrombosis imaging can be used for evaluating clotting components in a flexible, quantitative, data-rich, and cost-effective manner.

Supplementary Material

Refer to Web version on PubMed Central for supplementary material.

Acknowledgments

The author is grateful to Dr. Haig Kazazian for supplying the Factor VIII knockout mice, Dr. David Ginsburg for supplying the Factor V Leiden mice, and Dr. Marschall Runge for providing the anti-fibrin hybridoma cell line.

Sources of Funding: This work was supported by NIH grant EB007582.

References

1. Fay WP, Parker AC, Ansari MN, Zheng X, Ginsburg D. Vitronectin inhibits the thrombotic response to arterial injury in mice. Blood. 1999; 93:1825–1830. [PubMed: 10068653]
2. Kawasaki T, Kaida T, Vermylen AJ, Hoylaerts MF. A new animal model of thrombophilia confirms thaqt high plasma factor VIII levels are thrombogenic. Thrombos Haemostas. 1999; 81:306–311.
3. Matsuno H, Kozawa O, Niwa M, Ueshima S, Matsuo O, Collen D, Uematsu T. Differential role of components of the fibrinolytic system in the formation and removal of thrombus induced by endothelial injury. Thrombos Haemostas. 1999; 81:601–604.
4. Denis C, Methia N, Frenette PS, Rayburn H, Ullman-Cullere M, Hynes RO, Wagner DD. A mouse model of severe von Willebrand disease: defects in hemostasis and thrombosis. Proc Natl Acad Sci USA. 1998; 95:9524–9529. [PubMed: 9689113]
5. Rosen ED, Raymond S, Zollman A, Noria F, Sandoval-Cooper M, Shulman A, Merz JL, Castellino FJ. Laser-induced noninvasive vascular injury models in mice generate platelet- and coagulation-dependent thrombi. Am J Pathol. 2001; 158:1613–1622. [PubMed: 11337359]
6. Falati S, Gross P, Merrill-Skoloff G, Furie BC, Furie B. Real-time in vivo imaging of platelets, tissue factor and fibrin during arterial thrombus formation in the mouse. Nat Med. 2002; 8:1175–1181. [PubMed: 12244306]

7. Zimmermann R, Zeltsch C, Lange D. Estimation of thrombus formation by labeling of platelets, red cells and fibrinogen in experimental thrombosis. Thrombos Res. 1979; 16:147–158.
8. Shoenfeld NA, Yeager A, Connolly R, Ramberg K, Forgione L, Giorgio A, Valeri CR, Callow AD. A new primate model for the study of intravenous thrombotic potential and its modification. J Vasc Surg. 1988; 8:49–54. [PubMed: 2455070]
9. Hui KY, Haber E, Matsueda GR. Monoclonal antibodies to a synthetic fibrin-like peptide bind to human fibrin but not fibrinogen. Science. 1983; 222:1129–1131. [PubMed: 6648524]
10. Runge MS, Bode C, Matsueda GR, Haber E. Antibody-enhanced thrombolysis: Targeting of tissue plasminogen activator in vivo. Proc Natl Acad Sci USA. 1987; 84:7659–7662. [PubMed: 3118374]
11. Cooley BC, Szema L, Chen CY, Schwab JP, Schmeling G. A murine model of deep vein thrombosis: characterization and validation in transgenic mice. Thrombos Haemostas. 2005; 94:498–503.
12. Maxwell MJ, Dopheide SM, Turner SJ, Jackson SP. Shear induces a unique series of morphological changes in translocating platelets: effects of morphology on translocation dynamics. Arterioscler Thromb Vasc Biol. 2006; 26:663–669. [PubMed: 16385083]
13. Nesbitt WS, Westein E, Tovar-Lopez FJ, Tolouei E, Mitchell A, Fu J, Carberry J, Fouras A, Jackson SP. A shear gradient-dependent platelet aggregation mechanism drives thrombus formation. Nat Med. 2009; 15:665–673. [PubMed: 19465929]
14. Koster T, Rosendaal FR, de Ronde H, Briet E, Vandenbroucke JP, Bertina RM. Venous thrombosis due to poor anticoagulant response to activated protein C: Leiden thrombophilia study. Lancet. 1993; 342:1503–1506. [PubMed: 7902898]
15. Bertina RM, Koeleman BPC, Koster T, Rosendaal FR, Dirven RJ, de Ronde H, et al. Mutation in blood coagulation factor V associated with resistance to activated protein C. Nature. 1994; 369:64–67. [PubMed: 8164741]
16. Cui J, Eitman DT, Westrick RJ, Christie PD, Xu ZJ, Yang AY, et al. Spontaneous thrombosis in mice carrying the Factor V Leiden mutation. Blood. 2000; 96:4222–4226. [PubMed: 11110695]
17. Crafoord C. Preliminary report of post-operative treatment with heparin as a preventive of thrombosis. Acta Chir Scand. 1937; 79:407–426.
18. Murray DWG, Jaques LB, Perrett TS, Best CH. Heparin and the thrombosis of veins following injury. Surgery. 1937; 2:163–187.
19. Friedman M, Van den Bovenkamp GJ. The pathogenesis of a coronary thrombus. Am J Pathol. 1966; 48:19–44. [PubMed: 5902836]
20. Sevitt S. The structure and growth of valve-pocket thrombi in femoral veins. J Clin Pathol. 1974; 27:517–528. [PubMed: 4138834]

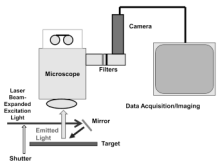

Figure 1.

Schematic of imaging system, showing beam-expanded, shuttered, laser excitation light with downward (mirror) reflection to illuminate the surgical field (target), and subsequent emitted light passing through an operating microscope, with filter wheel emission-specific capture by a monochrome camera and image data acquisition.

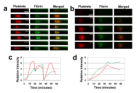

Figure 2.

Representative images are shown from time-lapse videos of platelets (labeled with Vybrant DiD, shown in red) and labeled fibrin (antibody specific for fibrin, labeled with Alexa-Fluor-532, shown in green) and merged images, for the arterial (a) and venous (b) electrolytic injuries. Colorization has been added and relative intensities have been modified from the original monochrome camera capture format; all images within a given vertical column of panels have identical intensity adjustment. Note massive embolism seen after 37 minutes in the arterial model (a). Flow is from left to right in the vessels; bars are 500 μm. Videos of the same clots for (a) and (b) can be viewed in the Supplemental Videos 1 and 2, respectively. Relative background-subtracted platelet (red lines) and fibrin (green lines) image intensities are shown graphically, measured every 2 minutes, for the clot regions of the arterial (c) and venous (d) electrolytic injuries used in (a) and (b), respectively.

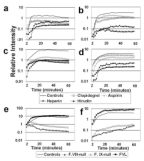

Figure 3.

Intensity-normalized temporal profiles are shown of clot regions for arterial (a, b) and venous (c, d) electrolytic injury models under the influence of various clot-inhibiting compounds, with quantification of normalized intensities within evident clotting regions (arbitrary units) for platelets (a, c) and anti-fibrin (b, d). Antithrombotic compounds: heparin (200 units/kg), hirudin (1 mg/kg), aspirin (15 mg/kg), and clopidogrel (10 mg/kg); controls are vehicle-treated. All compounds were used at presumed high therapeutic-dose equivalence for mice. Similar normalized profiles for venous electrolytic injuries, without antithrombotic therapies, are shown for Factor VIII and IX knockout and Factor V Leiden transgenic mouse lines, with graph image capture for platelets (e) and fibrin (f) accumulation. Normalized intensities are displayed on a logarithmic scale on the y-axis in all graphs. Each line represents the average of 4-8 experimental thrombus inductions, with one thrombus per mouse.